



Research papers

Small Arctic rivers mapped from Sentinel-2 satellite imagery and ArcticDEM

Xin Lu^a, Kang Yang^{a,b,c,*}, Yao Lu^a, Colin J. Gleason^d, Laurence C. Smith^{e,f,g}, Manchun Li^{a,b}^a School of Geography and Ocean Science, Nanjing University, Nanjing 210023, China^b Jiangsu Provincial Key Laboratory of Geographic Information Science and Technology, Nanjing 210023, China^c University Corporation for Polar Research, Beijing 100875, China^d Department of Civil and Environmental Engineering, University of Massachusetts, Amherst, MA 01002, USA^e Institute at Brown for Environment and Society, Brown University, Providence, RI 02912, USA^f Department of Earth, Environmental and Planetary Sciences, Brown University, Providence, RI 02912, USA^g Department of Geography, University of California, Los Angeles, Los Angeles, CA 90095, USA

ARTICLE INFO

ABSTRACT

Keywords:

Small rivers
River network mapping
Sentinel-2
Landsat
ArcticDEM
Arctic

Small rivers (< 30 m) are significant components of terrestrial river networks and remote sensing is a necessary tool to study them at the global scale. However, current global hydrography data products generally include only rivers that are wider than 30 m, neglecting smaller waterways and thus limiting our understanding of surface water processes, especially in remote areas. We present a new automated methodology to map two Arctic actively-flowing river networks (Kotuy and Coleen Rivers, with study areas of $\sim 12,000$ km 2 and 10,000 km 2 , respectively), including small rivers as narrow as 10 m from Sentinel-2 multispectral satellite imagery and high-resolution ArcticDEM digital elevation data. First, preliminary river network masks were generated by using Gabor filtering and path opening morphological operations on Normalized Difference Water Index (NDWI) images. Second, ArcticDEM data were employed to simulate surface flow paths, and the resultant drainage networks were used to create river areas of interest (AOI) and subsequently eliminate non-water features outside the river AOI. Third, gaps along remotely sensed small river channels were filled using the ArcticDEM-modeled drainage networks, yielding continuous river networks with high spatial resolution. We compared the 10 m Sentinel-ArcticDEM merged River Network (SARN) with the National Hydrography Dataset (NHD) and four 30 m Landsat-derived hydrography data products (GSW, GRWL, FROM-GLC 2017, and G3WBM). We conclude: (1) SARNs have similar quality to the > 1st order NHD ($> 70\%$ of NHD streams appear in SARNs). (2) At a reach scale, SARNs include more small rivers with the drainage densities at least ~ 4.5 times larger than Landsat-derived hydrography data products. Similarly, coupling ArcticDEM data with 30 m Landsat satellite images increases resultant drainage densities approximately three-fold. (3) At a catchment scale, merging remotely sensed river networks with ArcticDEM-modeled drainage networks significantly improves river connectivity (defined as the longest connected river length) with at least a ten-fold increase over the other hydrography data products examined here. In sum, merging high-resolution Sentinel-2 imagery with ArcticDEM data enable effective, continuous mapping of complex fluvial drainage patterns of Arctic rivers.

1. Introduction

Terrestrial river networks transport and store large quantities of alluvial material, and drive climate and ecosystems via biogeochemical cycles (Jung et al., 2010; Raymond et al., 2013; Sjögersten et al., 2014; Vorosmarty, 2000). Small river ecosystems tend to be particularly variable over time and have frequent land-atmosphere interactions (Allen et al., 2018; Benstead and Leigh, 2012; Meyer et al., 2007; Peterson, 2001). For example, during wet periods, river network drainage density (D_d , the ratio of river length to the total area for a given

catchment) may be over eight times greater than during periods with normal water levels (Benstead and Leigh, 2012). Moreover, 50% of global greenhouse gas emissions originate from small rivers and streams (Allen et al., 2018; Butman et al., 2016). Therefore, neglecting small rivers in global analyses could underestimate the role that river networks play in the biogeochemical cycle, and accurate mapping of river networks is needed.

The Arctic region contains most of the global rivers and lakes (Allen and Pavelsky, 2018; Pekel et al., 2016; Yamazaki et al., 2015). These rapidly respond to regional water balance and surface-groundwater

* Corresponding author at: School of Geography and Ocean Science, Nanjing University, Nanjing 210023, China.

E-mail address: yangkangju@gmail.com (K. Yang).

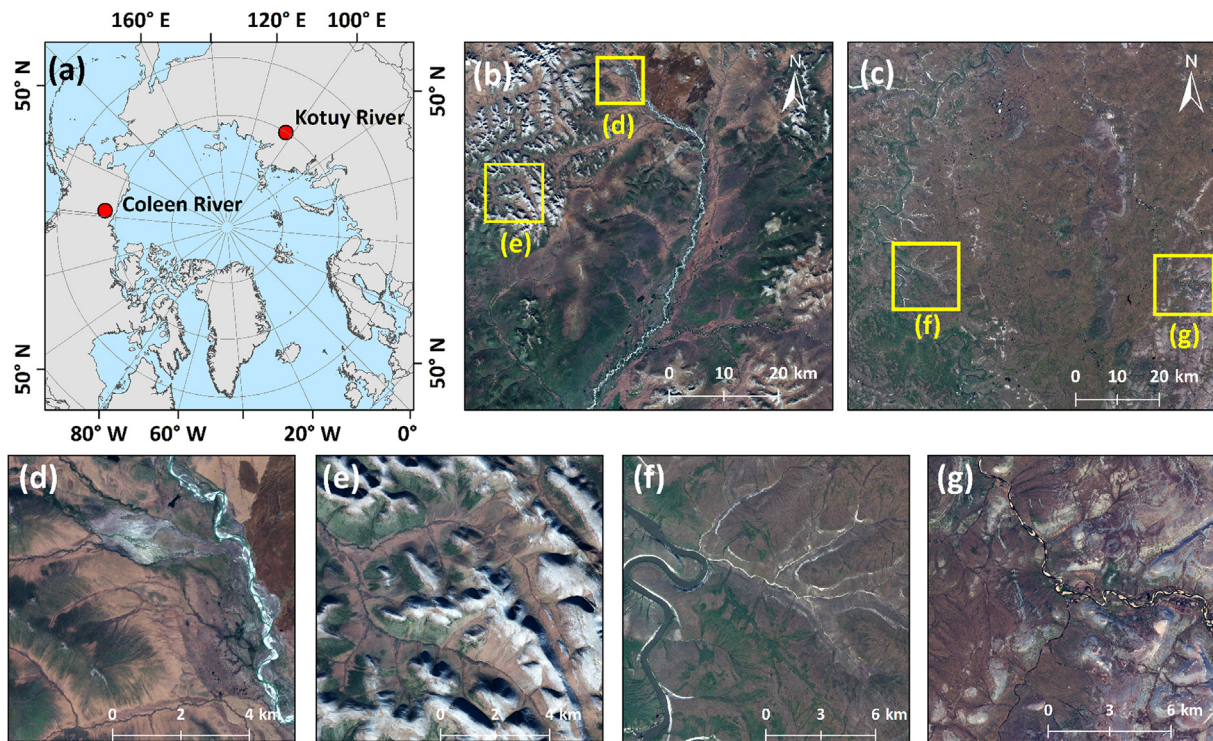


Fig. 1. (a) Location of study areas. (b) Sentinel-2B satellite image of the Coleen River, Alaska (acquired on September 17, 2017, RGB: bands 4 (Red), 3 (Green), 2 (Blue)). (c) Sentinel-2A satellite image of the Kotuy River, Russia (acquired on June 18, 2016, RGB: bands 4 (Red), 3 (Green), 2 (Blue)). (d)–(g) are four typical sites in (b) and (c). (For interpretation of the references to colour in this figure legend, the reader is referred to the web version of this article.)

interactions, and these dynamics are shifting under recent climate change (Cooley et al., 2017; Cooley et al., 2019). Further, the Arctic is thought to be a major store of greenhouse gasses set to alter the global carbon budget as permafrost thaws and releases especially methane into the atmosphere (Raymond et al., 2013). Therefore, mapping Arctic river networks in particular is essential to better constrain diverse Arctic climatic and physiographic and physiochemical processes.

River drainage patterns have been traditionally mapped using land surveys, following the principle that streams flow down-gradient (i.e., downhill). For example, The National Hydrography Dataset (NHD) published by the United States Geological Survey (USGS) represents the surface water system of the United States, which was generated from detailed topographic maps (Simley and Carswell, 2009). Currently, most continuous drainage networks are commonly modeled from digital elevation models (DEMs) (Fairfield and Leymarie, 1991; O'Callaghan and Mark, 1984); examples include the widely used HydroSHEDS and HYDRO1K datasets (Lehner et al., 2006; USGS, 2001). This is analogous to the use of a topographical map, and successful DEM prediction of rivers enables a significant change in our understanding of global hydrology. However, some errors in DEMs, such as speckle noise, stripe noise, absolute bias, and tree height bias, distort the representation of drainage networks at the global scale (Yamazaki et al., 2017).

In addition to DEMs, satellite remote sensing has also been widely used in the mapping, analysis, and dynamic monitoring of actively-flowing river networks, building off traditional work using aerial surveys (Allen and Pavelsky, 2018; Alsdorf et al., 2007; Gleason and Smith, 2014; McCabe et al., 2017; Smith, 1997). Researchers have developed various global hydrography data products in an effort to understand rivers at the global scale. For example, Yamazaki et al. (2015) used multi-temporal Landsat images and an automated algorithm to produce the Global 3 arc-second Water Body Map (G3WBM). Gong et al. (2013) classified Landsat images and produced the 30 m Finer Resolution Observation and Monitoring-Global Land Cover 2017 (FROM-GLC 2017) map, which identified open water classes with relatively high

classification accuracy. Using Google Earth Engine and the entire Landsat archive, Pekel et al. (2016) processed over three million satellite images to create the 30 m Global Surface Water (GSW) dataset. The GSW quantified changes in the temporal and spatial distribution of global seasonal and permanent water bodies for 32 years (1984–2015), revealing long-term increases and decreases in global surface water extent. Allen and Pavelsky (2018) produced the 30 m Global River Widths from Landsat (GRWL) dataset, which includes continuous open water masks and river centerlines. The river and stream surface areas calculated by GRWL were $\approx 45\%$ larger than previous estimates, significantly advancing our knowledge of the extent and spatial distribution of surface water around the world.

These new global data products on surface water extent and river planforms have significantly improved current understanding of the Earth's hydrography at a reach scale. However, because they are derived from Landsat imagery and limited to rivers wider than 30 m, these miss abundant smaller rivers. At present, there are no free available remotely sensed hydrography data products with spatial resolutions finer than 30 m. There is therefore a knowledge gap in river hydrography that ends at 30 m width, which limits our understanding of the morphology and dynamic changes in small rivers and the processes of surface hydrology at a finer reach scale. As a result, field surveys are currently an important means of studying small rivers and streams for global hydrography work (e.g., Allen et al. (2018), Godsey and Kirchner (2014)). However, it is costly and impractical to carry out large-scale field surveys of entire river networks. We contend that there are now sensors and computational resources available to dramatically increase the scale of satellite-mapped river networks as well as small rivers.

In addition to the problem of resolution, rivers extracted from remotely sensed images are commonly fragmented and lack a proper topology. Fully connected river networks are required for quantitative analysis and hydrological modeling at a catchment scale (Czuba and Foufoula-Georgiou, 2015; Downing et al., 2012; Seybold et al., 2017), and thus current remote sensing techniques can fall short of this goal. In contrast, drainage networks modeled from DEMs are typically

Table 1
Comparison of hydrography data products.

River dataset	Data source	Resolution	Type	Notes	Reference
G3WBM (Global 3 arc-second Water Body Map) FROM-GLC 2017 (Finer Resolution Observation and Monitoring-Globa Land Cover, 2017)	Landsat	90 m 30 m	Water body Water body	Permanent and seasonal open water mask Land use and cover change product	Yamazaki et al. (2015) Gong et al. (2013)
GSW (Global Surface Water)	Landsat	30 m	Water body	Long-term permanent and seasonal open water mask	Pekel et al. (2016)
GRWL (Global River Widths from Landsat)	Landsat	30 m	Water body, river network	River width dataset (river width > 30 m)	Allen and Pavelsky (2018)
SARN/LARN (Sentinel/Landsat-ArcticDEM merged River Networks)	Sentinel-2/Landsat-8, ArcticDEM	10/30 m	Water body, river network	Continuous river networks with small rivers	This study

continuous, but have difficulty in predicting whether or not a free flowing river actually occupies a topographic low: just because a trough exists does not mean it contains a river. Therefore, integrating satellite imagery with DEMs should compensate for errors in connectivity and actual presence, and consequently generate accurate and continuous river networks that present actual river distributions.

To that end, we combine 10 m Sentinel-2 satellite imagery and a high-resolution DEM in order to map Arctic hydrologically continuous river networks with small rivers for Kotuy and Coleen Rivers, with study areas of ~12,000 km² and 10,000 km², respectively. Specifically, we use Gabor filtering and path opening morphological operations to extract actively-flowing rivers from Sentinel-2 images, and merge these with ArcticDEM-modeled drainage networks to remove non-water features and fill gaps along remotely sensed small river channels. Results show, as expected, that river networks derived from 10 m remotely sensed products are far more complete and continuous than those derived from 30 m products at reach and catchment scales, thus more accurately depicting actively-flowing river networks on the ground. We contextualize what this finer resolution network means for associated hydrology of the catchments, and give some recommendations for future research.

2. Data and study area

2.1. Remotely sensed datasets

The European Space Agency (ESA) launched Sentinel-2 satellites, comprised of a constellation of two satellites (Sentinel-2A and Sentinel-2B), in 2015 and 2017, respectively. The Sentinel-2 satellites have a large swath (290 km) and a frequent revisit period (five days). Both carry a single multi-spectral instrument (MSI) having 13 spectral bands in the visible (VIS), near infrared (NIR), and short wave infrared (SWIR) spectral domains with spatial resolutions ranging from 10 m to 60 m (Drusch et al., 2012). We used radiometrically and geometrically corrected Level-1C Sentinel-2 image products (Baillarin et al., 2012) free available from <https://earthexplorer.usgs.gov>.

ArcticDEM is a high-resolution, pan-Arctic topography dataset generated through stereo-photogrammetric processing of panchromatic images from WorldView-1/2/3 and GeoEye-1 satellites (Morin et al., 2016). ArcticDEM has a vertical precision of approximately 0.3 m (Dai et al., 2018), and in 2018, the Polar Geospatial Center (PGC) issued ArcticDEM Release 7 (<http://arcticdem.org>) covering all land areas north of 60°N. In addition to providing 2 m resolution strip DEMs, the PGC also selected high-quality 2 m strip DEM files to produce 2 m mosaic DEMs, in which void areas were reduced through re-mosaicking of the entire ArcticDEM domain. Reduced-resolution versions of the mosaic DEMs are also available at resolutions of 10 m, 32 m, 100 m, 500 m, and 1 km. This study used the 10 m ArcticDEM product, in order to match the spatial resolution of the Sentinel-2 satellite imagery and enhance data processing efficiency.

2.2. Study area

Two Arctic basins, the Kotuy and Coleen Rivers, were chosen as testbeds for the methodology presented here (Fig. 1). The Kotuy River Basin, located in Krasnoyarsk Krai in Russia, is a typical Arctic basin characterized by continuous permafrost, tundra vegetation and sparse human population (Bliss, 1981; Brown et al., 1997). The Coleen River Basin, located in the southern part of the Brooks Range in Alaska, is characterized by tundra and taiga vegetation, high topographic relief and continuous permafrost with high ground ice content and thick overburden (Brabets et al., 2000; Brown et al., 1997). Both basins are covered with snow and ice for 7–8 months of each year. Ice and snowmelt in these two study areas lasts from June until September (Ala-Aho et al., 2018; Anderson et al., 2013; Chen et al., 2014) and their streamflow typically peaks in mid-June (Brabets et al., 2000;

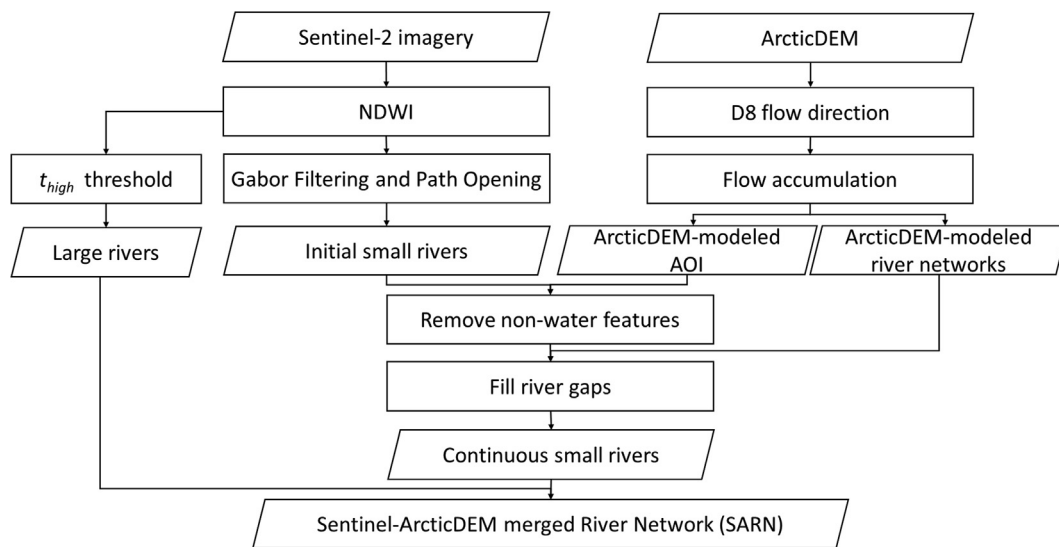


Fig. 2. Methodological flow chart of extracting river networks by merging Sentinel-2 satellite imagery with the high-resolution ArcticDEM data.

Shiklomanov et al., 2002).

These basins have well-developed river networks and widely distributed small rivers (Fig. 1). Basin areas are $\sim 12,000 \text{ km}^2$ and $10,000 \text{ km}^2$ for the Kotuy and Coleen Rivers, respectively. We selected a cloudless Sentinel-2B image acquired on June 18, 2016 (L1C tile number: T48WVC) for the Kotuy River to represent its peak streamflow. For the Coleen River, no cloudless Sentinel-2 images are available in June; thereby, a Sentinel-2A image acquired on September 17, 2017 (L1C tile number: T07WDR) was used to study the Coleen River.

2.3. Datasets for river network comparison

The Landsat-derived GSW, GRWL, FROM-GLC 2017, and G3WBM global hydrography datasets were chosen for comparison with the river networks produced in this study (Table 1). For the Coleen River, the NHD was also used for validation of rivers. The NHD (<https://nhd.usgs.gov/>) includes all natural and anthropogenic water bodies mapped at a scale of 1:24 000 or better (Simley and Carswell, 2009), and represents the most comprehensive and comparative dataset for validation of satellite-derived water maps (Yamazaki et al., 2015).

The GSW (Pekel et al., 2016) maps open water changes at a global scale over a period of 32 years (1984 – 2015), including water occurrence and change intensity, water seasonality (October 2014 – October 2015), and annual water recurrence. This study utilized maximum water extent data from October 2014 to October 2015. The official FROM-GLC website (<http://data.ess.tsinghua.edu.cn/>) has recently released 2017 Global Land Cover product, which separates “Water” and “Wetland” classifications. The “Water” classification includes natural and artificial waterbodies. The “Wetland” classification mainly includes inundated marsh land with emergent vegetation and wet muddy bare land such as a wet lake bottom (Gong et al., 2013). We merged these two classifications to obtain the FROM-GLC 2017 water extent data. The GRWL dataset (Allen and Pavelsky, 2018) extracts rivers at mean annual discharges from Landsat images to build global open water masks and river width products. The G3WBM dataset (Yamazaki et al., 2015) contains distributions of permanent and temporal water bodies mapped in 1990, 2000, 2005, and 2010. The open water data from the four years were combined to obtain the maximum water extent data.

In sum, we have obtained river locations and surface areas from a variety of products for comparison with our proposed method. All of these products are Landsat based and global save for the NHD. We consider the NHD as a ‘gold standard’ for comparison, but also note issues of stream migration between the creation of NHD for the Coleen

Rivers before 1973 and our study made 40 years later in this highly dynamic environment.

3. Methods

3.1. Sentinel-2 river network extraction

Small and large rivers were extracted separately in this study (Fig. 2). Since river channels in the raw Sentinel-2 imagery are not easily delineated from visual inspection (Fig. 3a), we calculated the Normalized Difference Water Index (NDWI) (McFeeters, 1996) to enhance the appearance of all liquid water bodies in each Sentinel-2 satellite image (Fig. 3b). Larger rivers were then extracted using a NDWI threshold of 0.1 following Yang et al. (2014). However, low spectral contrast between smaller rivers and surrounding land made small rivers difficult to discern using this threshold, which agrees with results obtained by Cooley et al. (2017) and Feng et al. (2019). To improve detection of small rivers, we followed the method of Yang et al. (2015) to increase the contrast between small rivers and the image background. This method used a band-pass filter ramped between $1/200 \text{ m}^{-1}$ and $1/40 \text{ m}^{-1}$ to remove low-frequency background and high-frequency noise (Fig. 3c), thus enhancing detection of smaller rivers. However, even after band-pass filtering, smaller rivers still exhibit low spectral contrast with the image background. A Gabor filter was applied to enhance the cross sectional features of small rivers with width less than two pixels (Fig. 3d). A parsimonious path opening (PPO), which is a longitudinal-direction path operator, was then used to enhance the connectivity of rivers > 20 pixels (200 m) in length (Fig. 3e). These three steps enhanced the linear features of the images and improved the connectivity and completeness of the extracted river networks. Through trial and error and visual comparison with each original Sentinel-2 image, a global threshold of 20 (i.e., 20 out of 255 in an 8-bit image) was then determined to produce binary open water masks (Fig. 3f). These open water masks are simply pixels we define as water and non-water, and additional processing is needed to transform these into objects recognized programmatically as river channels. Sentinel-2 river network centerlines were thus produced using the ArcScan tool (Bajjali, 2018a) from the open water masks.

3.2. ArcticDEM drainage network modeling

The above processing produced initial river networks, but some patchy, misidentified features (e.g., mountain shadows) remained in

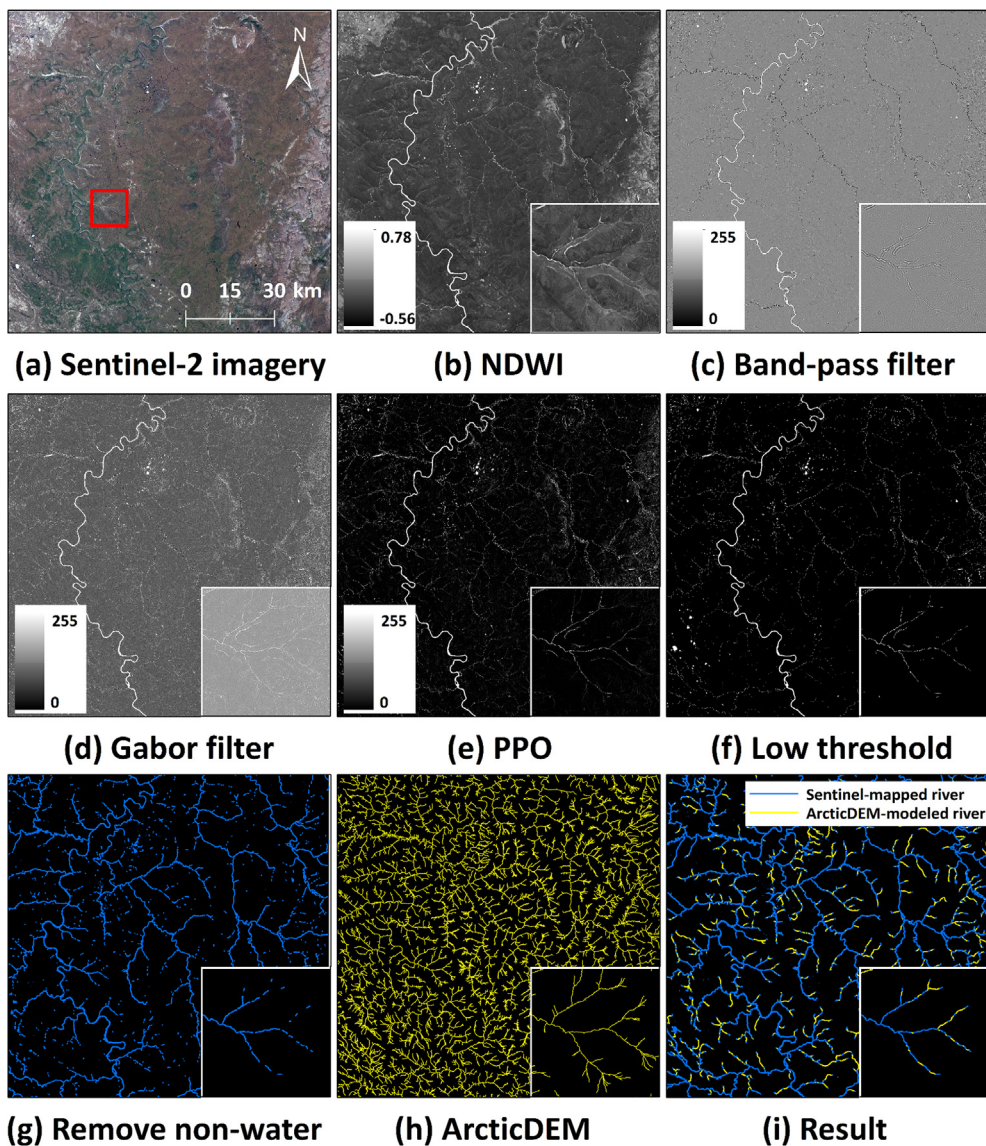


Fig. 3. Workflow for our proposed method. (a) Raw Sentinel-2 image of Kotuy River Basin; (b) Derivative NDWI image; (c) Band-pass filter of (b); (d) Application of Gabor filter; (e) Application of PPO algorithm; (f) Binary river mask (threshold $T = 20$); (g) Filtering of non-water features using ArcticDEM-modeled river areas of interest; (h) ArcticDEM-modeled drainage network ($A_c = 0.5 \text{ km}^2$, or 5000 pixels); (i) The final result of SARN.

our derived river networks. It is difficult to remove these effectively using a single threshold, because mountains and clouds obscure the spectral properties of water bodies, and shadows have NDWI values similar to those of water bodies (Feyisa et al., 2014; Verpoorter et al., 2012). Additionally, Xu (2005) discovered that bare land and water bodies have practically identical spectral characteristics in the green and near-infrared bands, making NDWI-based water extraction less effective in the Arctic tundra. Moreover, additional gaps appear in the Sentinel-mapped river networks because we utilized pixel-based river extraction methods instead of object based methods. Therefore, it is necessary to remove non-water features and fill the gaps in the Sentinel-mapped river networks to obtain more accurate and continuous river extraction results. This is a known problem for river networks derived from satellite images we highlight in the introduction, and thus we merged the power of DEMs and satellite imagery to address this problem.

The first step in producing DEM-based stream networks is to produce a flow accumulation map. In this study, a high-resolution flow accumulation map was produced from ArcticDEM through a sequence of sink filling, D8 flow direction calculation, and flow accumulation

calculation using hydrologic analysis tools in ArcGIS (Bajjali, 2018b). The density of the resulting drainage networks are controlled almost exclusively by the choice of the accumulation area threshold, the theoretical land surface area needed to produce an open-water river (Li and Wong, 2010). This translates to the size of the smallest sub-watershed within the basin where streams generation begins. A lower area threshold (i.e., smaller sub-watersheds) will create denser river features to the point where some streams may be too small to actually exist, whereas a higher area threshold will reduce the number of river features, neglecting some small streams. For this reason, DEM-modeled drainage networks are generally not in consistent with the actual distribution of actively-flowing surface water (Kenward, 2000; Yang et al., 2015). Therefore, in order to determine the river areas of interest (i.e., potential actively-flowing river locations), we chose an accumulation area threshold ($A_c = 0.5 \text{ km}^2$, or 5000 pixels) to produce an ArcticDEM-modeled drainage network that would cover the entire Sentinel-mapped river networks (Fig. 3h).

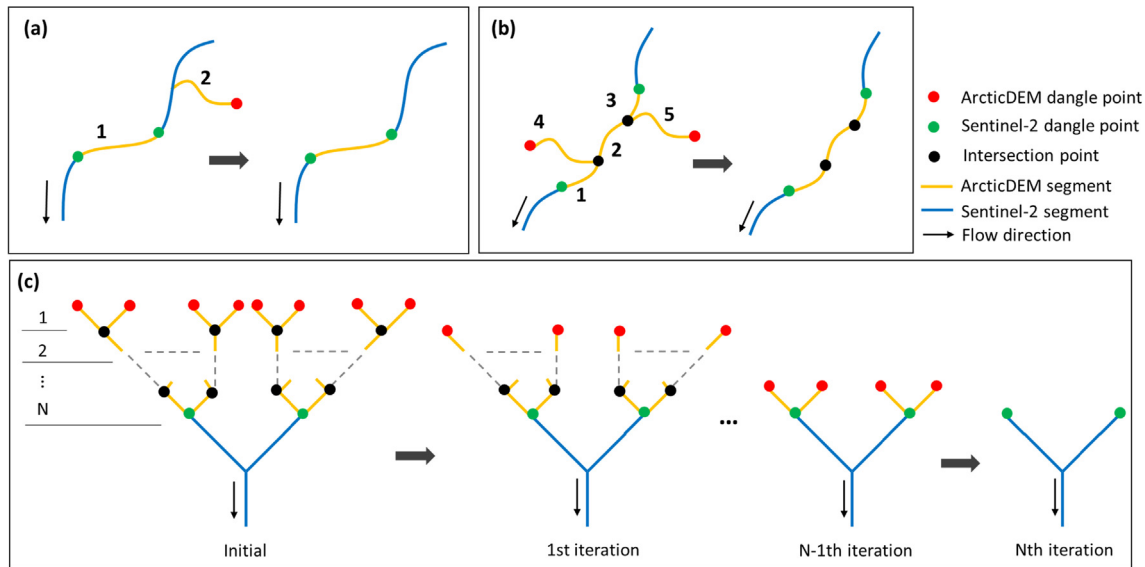


Fig. 4. Three spatial relationships exist between Sentinel-mapped rivers and ArcticDEM-modeled rivers: (a) A single DEM segment connects to a Sentinel-2 gap segment; (b) Multiple DEM segments connect to a Sentinel-2 gap segment; (c) N order dangling DEM segments connect to Sentinel-2 terminal segments.

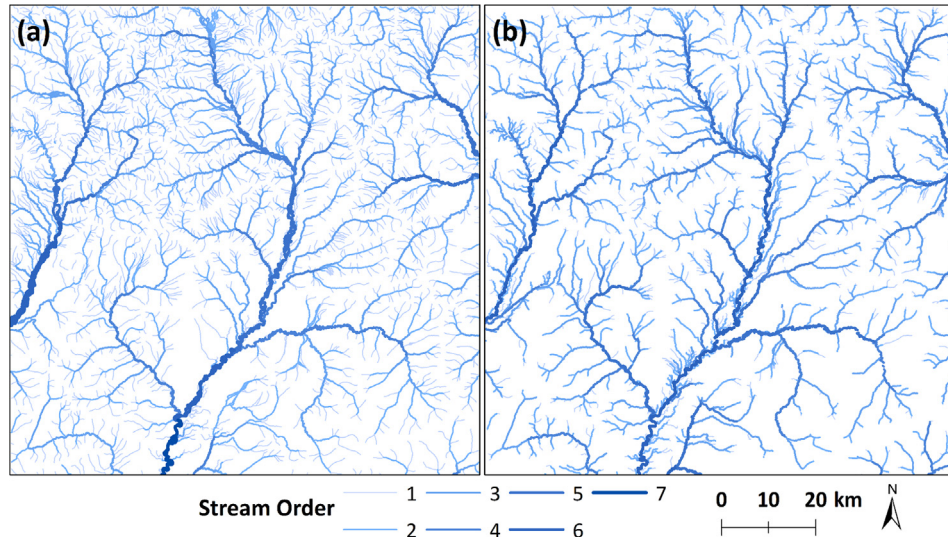


Fig. 5. Comparisons of Coleen river networks derived from (a) NHD and (b) SARNs.

Table 2

Statistics of the proportion of the SARNs consistent for NHD under each stream order.

Stream order	Total river length of NHD (km)	NHD appears in the 50-m SARN buffer	
		River length (km)	Proportion (%)
1	4091	1324	32.4
2	1564	1121	71.7
3	1080	862	79.8
4	563	406	72.1
5	284	154	54.3
6	187	75	39.8
7	33	12	37.5
> 1	3711	2629	70.9
All	7802	3954	50.7

Table 3

Summary statistics of D_d , OWF and L_{max} for the Coleen and Kotuy Rivers as derived from SARNs/LARNs and five other hydrography data products.

Rivers	Hydrography products	D_d (km^{-1})	OWF (%)	L_{max} (km)
Coleen	Kotuy	0.337	0.99	2512
	SARNs	0.222	1.42	1492
	LARNs	0.069	0.94	251
	GSW	0.054	0.74	428
	GRWL	0.050	0.71	83
	FROM-GLC 2017	0.037	0.63	199
	G3WBM	0.571	1.24	2876
	SARNs	0.364	2.06	1659
	LARNs	0.795	–	3906
	NHD	0.079	0.68	295
Kotuy	GSW	0.024	0.17	170
	GRWL	0.063	0.46	98
Coleen	FROM-GLC 2017	0.047	0.78	24
	G3WBM			

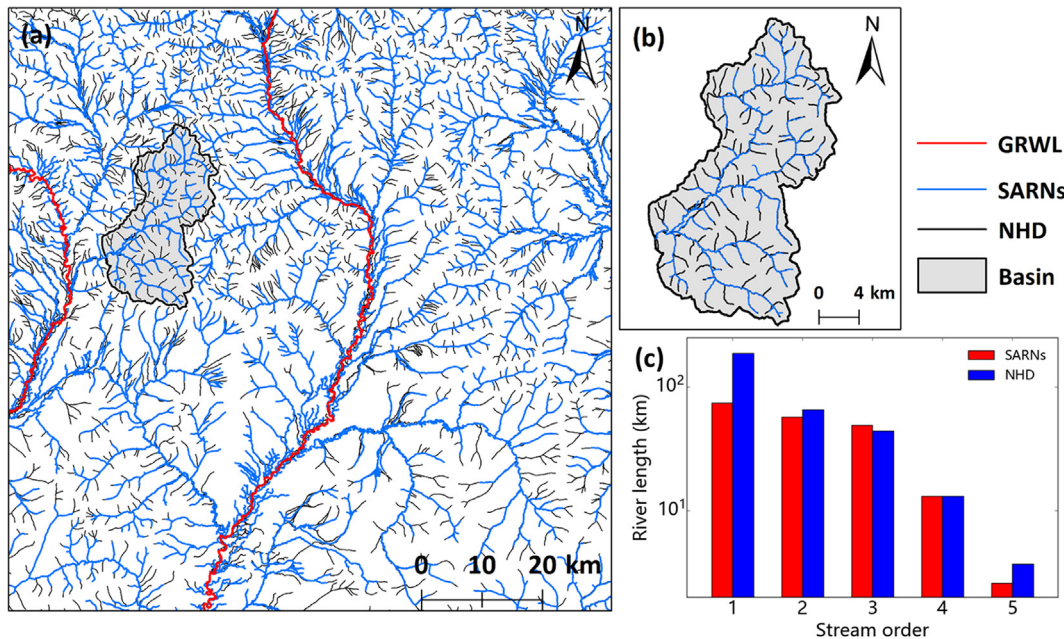


Fig. 6. Analysis river networks at the catchment scale. (a) is the river distributions of SARNs, NHD and GRWL in Coleen River Basin, (b) is the river distributions of SARNs and NHD in a 331-km² sub-basin of the Coleen River. (c) is comparisons of river lengths of SARNs and NHD by stream order.

3.3. Sentinel-2 and ArcticDEM river network merging

From visual inspection, river networks extracted from Sentinel-2 images accurately reflected the real-world drainage patterns of the Kotuy and Coleen Rivers, but some gaps in the river networks remained. In contrast, drainage networks modeled from ArcticDEM were continuous, but did not always accurately determine actively-flowing rivers. Therefore, to obtain accurate and continuous river networks, we combine both of these derived river networks.

Our first step was to correctly co-locate rivers from both datasets, to do so, we created ArcticDEM-modeled areas of interest (AOI), by buffering five pixels (50 m) in width to remove non-water features. Water bodies from the Sentinel-mapped open water mask were considered to be correctly extracted if they fell inside the ArcticDEM-modeled AOI, and to be incorrectly extracted if they fell outside. Some erroneously classified water features or small lakes could fall in the low-order river AOI; therefore, based on the fact that the length of such non-water features are generally short (< 300 m), in order to ensure the accuracy of the Sentinel-mapped river networks, any segment less than 300 m was removed (Fig. 3g).

Second, we merged ArcticDEM-modeled drainage networks with Sentinel-mapped river networks to connect gaps in remotely sensed river channels (Fig. 3g). Before connecting the river gaps, we identified three spatial relationships between the Sentinel-mapped river networks and DEM-modeled drainage networks (Fig. 4). (1) A DEM segment (Segment 1 in Fig. 4a) that increases network connectivity by connecting the two dangle points of a Sentinel-2 gap segment should be retained, while a DEM section that forms a tributary (Segment 2 in Fig. 4a) should be removed. (2) DEM segments aligned with and connected to a Sentinel-2 gap segment (Segments 1 and 3 in Fig. 4b) should be kept, while segments un-connected to a gap segment (Segments 2, 4, and 5 in Fig. 4b) should be retained only if they increase network connectivity (Segment 2 in Fig. 4b). (3) DEM segments that are connected to terminal segments of the Sentinel-mapped river networks and could produce extra n-order river segments should be removed (Fig. 4c).

Based on the above spatial relationships, we designed an iterative method for deleting redundant DEM segments (Fig. 4). River segment vertices were classified into three types: Sentinel-2 dangle point, DEM

dangle point, and intersection point (Fig. 4). Each DEM segment that should be deleted contained a single DEM dangle point. Therefore, we considered such DEM dangle points as the basis for deleting redundant DEM segments iteratively. With each iteration of the algorithm, only the lowest-order dangling DEM segments were deleted, so that the DEM-modeled drainage network became stripped of many redundant segments after the first iteration (Fig. 4a and b). However, redundant N-1 order DEM segments still remained attached to the Sentinel-2 segments (Fig. 4c) because these DEM segments formed a dendritic network and cannot be removed from a single iteration. Therefore, in this study, the lowest order of dangling DEM segments was removed iteratively until no further changes were made to the total length of the coupled river network; that is, until all of the extra DEM segments were removed (Fig. 4c). The described sequence of processing steps produced a final continuous and complete Sentinel-ArcticDEM merged River Network (SARN), which exhibits a classic dendritic fluvial drainage pattern (Fig. 3i). The presented SARN methodology was implemented using MATLAB and Python, and has been published on the GitHub platform (<https://github.com/njuRS>).

3.4. River morphometric metrics and comparison methodology

The motivation for our method lies in its improved spatial resolution, but this improved resolution only becomes relevant when deriving river morphometry and other quantities of hydrologic interest. Thus, a comparison between our method and the global Landsat products mentioned is in order to elucidate the differences therein. In addition, we tested our method using Landsat data to determine how our method performed against other mapping techniques (i.e., the global products) using the same data. We obtained Landsat-8 images captured in July 22, 2016 (Coleen River) and August 6, 2017 (Kotuy River) to delineate Landsat-ArcticDEM merged river networks (LARNs) for this purpose. Finally, the NHD is recognized as the official record of river location by the USGS, and we can use this dataset to compare our method against this government-issue dataset for the Coleen basin.

To quantitatively compare the hydrologic impact of our SARNs with the global products, LARNs, and NHD, we calculated five morphometric statistics metrics for each. These include drainage density (D_d , the ratio of river length to the total area for a given catchment), open water

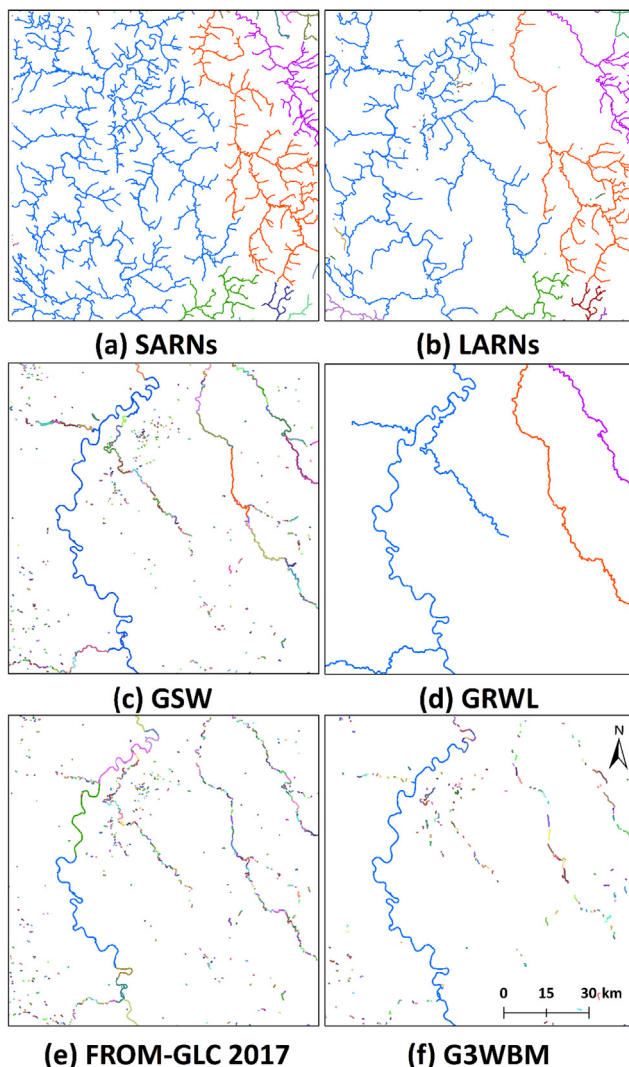


Fig. 7. Comparing actively-flowing river networks of (a) SARNs and (b) LARNs in Kotuy River, Russia with existing hydrography data products (c) GSW, (d) GRWL, (e) FROM-GLC 2017, and (f) G3WBM. A connected river network is in one certain color.

fraction (OWF, the ratio of water pixels to the total number of pixels), river connectivity (L_{max} , the longest connected river length), and river width. We used ArcScan to obtain river centerlines and calculate mean river widths for SARNs, LARNs, GSW, FROM-GLC 2017, and G3WBM datasets, which do not include widths. GRWL includes estimates of width.

To analyze the consistency of SARNs with NHD, we used a positional accuracy measure proposed by Goodchild and Hunter (1997) (computing the proportion of one linear feature length that lies within a buffer of another linear feature), and calculated the proportion of NHD appearing in SARNs buffer of width 50 m by stream order. Thus, we attempt to ensure that NHD and SARNs are producing rivers in the same location, in addition to comparing the metrics introduced above. Because the NHD does not include stream order values, we used the automated stream ordering tool in Geomorphic Network and Analysis Toolbox (GNAT, <https://gnat.riverscapes.xyz/index>), an ArcGIS Python Toolbox, to label Strahler stream orders (Strahler, 1957) for the NHD. Strahler stream ordering begins at order 1 for the smallest river and increases to number n , depending on how many stream junctions are observed in the basin. We also projected Strahler stream orders of the ArcticDEM-modeled drainage networks onto SARNs of the Coleen River (in Alaska) by creating a 100-m buffer area.

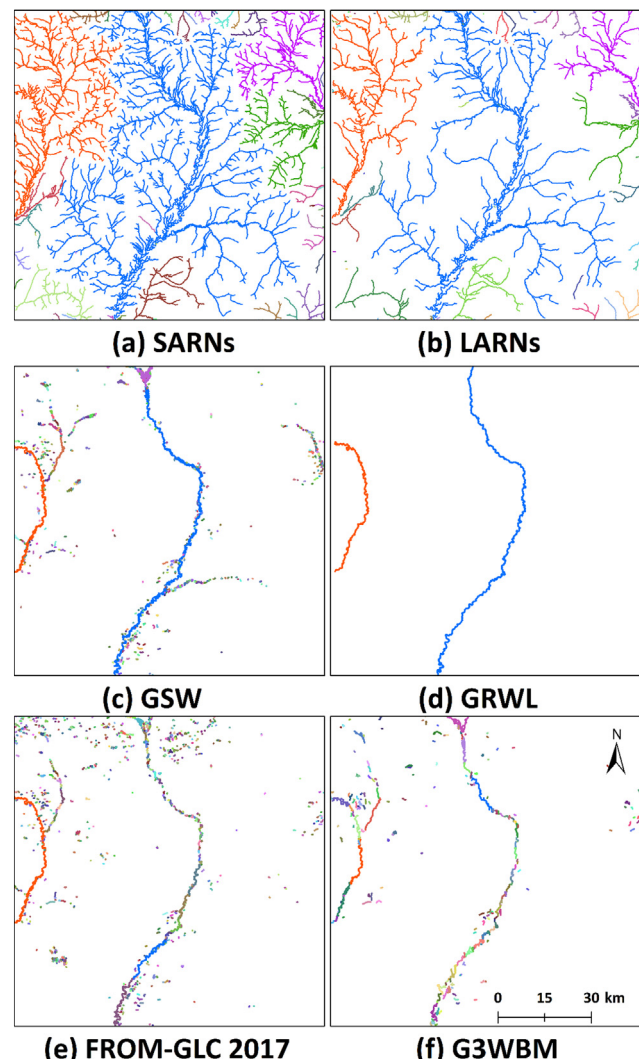


Fig. 8. Comparing actively-flowing river networks of (a) SARNs and (b) LARNs in the Coleen River, Alaska with existing hydrography data products (c) GSW, (d) GRWL, (e) FROM-GLC 2017, and (f) G3WBM. A connected river network is in one certain color.

4. Results

4.1. Comparison of SARNs with NHD

SARNs are able to accurately model larger than 1st order NHD, as > 70% of NHD appear in a SARN buffer of width 50 m. 1st order NHD are captured less well as 68% of NHD rivers do not appear within this 50 m buffer (Fig. 5 and Table 2). This performance is encouraging, as NHD contains rivers much smaller than represented by our flow accumulation threshold. Additionally, SARNs have D_d that is 71% of NHD and L_{max} that is 73% of the NHD (Table 3).

In addition to analyzing rivers at the reach scale, we selected a sub-basin (331-km²) of the Coleen River to compare SARNs with NHD at the catchment scale (Fig. 6a and b). The SARN method extracts numerous small rivers, and the sum river lengths of rivers of orders 2–4 are comparable to their NHD counterparts (Fig. 6c). In contrast, the sum length of 1st order SARNs is ~60% shorter than that of 1st NHD, while the sum length of 5th order SARNs is ~30% shorter. This is because higher-resolution NHD captures more < 10 m rivers and its high-order large rivers are more braided. Additionally, the sum river lengths of both SARNs and NHD are negatively correlated with stream order (Fig. 6c), which is consistent with a previous study (Downing et al.,

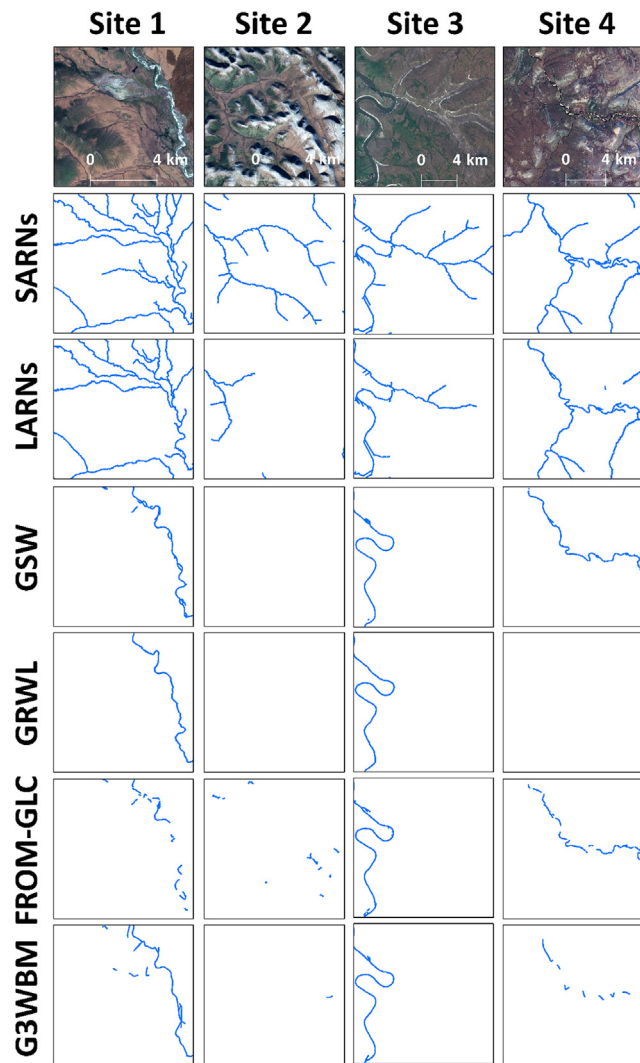


Fig. 9. Comparison of river networks derived from presented SARN method with four hydrography data products in four typical sites of Fig. 1.

2012).

4.2. Drainage density analysis

Due to the finer spatial resolution of both Sentinel-2 satellite images and ArcticDEM, SARNs are more continuous and contain more small rivers than the GSW, GRWL, FROM-GLC 2017, and G3WBM global datasets (Figs. 7–9). Estimated D_d values of the Kotuy and Coleen Rivers are 0.34 km^{-1} and 0.57 km^{-1} , respectively, and these are 4.8 and 7.2 times greater, respectively, than the largest D_d value of the other four hydrography data products, but less than NHD (Fig. 10, and Table 3).

Our method applied to Landsat (LARNs) also delineates a greater number of complete river networks (Figs. 7–9). For example, D_d values of the LARNs of Kotuy and Coleen Rivers are at least 3.2 and 4.6 times greater, respectively, than corresponding values for the four other Landsat-derived hydrography data products (Fig. 10 and Table 3). Therefore, existing hydrography datasets derived from Landsat imagery could detect much smaller rivers if merged with DEMs.

Amongst these existing hydrography data products, the GSW yields a slightly higher D_d than the other datasets (Fig. 10 and Table 3), consistent with a previous study (Aires et al., 2018). However, in areas covered with bare land and mountain shadows, the GSW produces poor results (Figs. 7c, 8c and 9), as do the FROM-GLC 2017 (Figs. 7e, 8e, and 9). The GRWL-based D_d in the Coleen River is lower than that in the

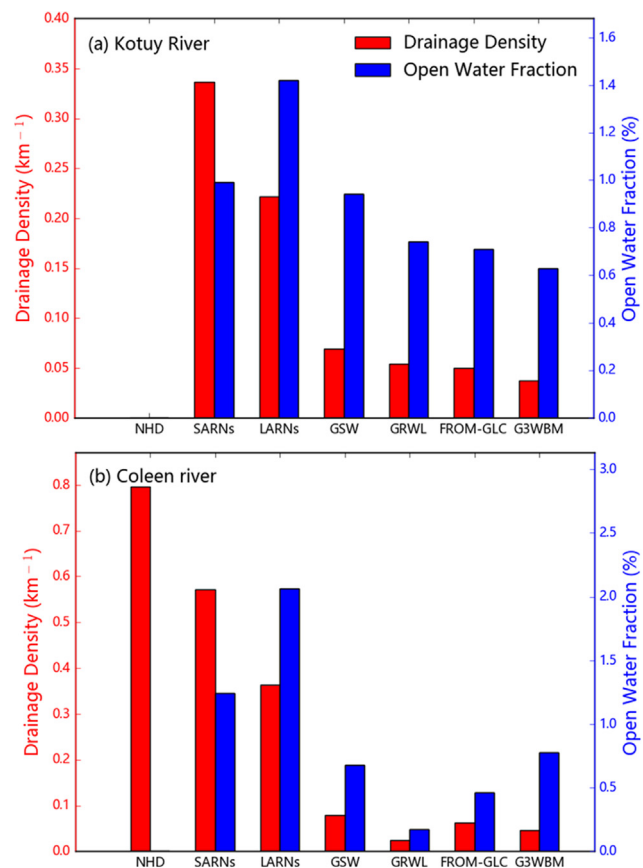


Fig. 10. Drainage density (D_d) and Open Water Fraction (OWF) comparisons between the resultant river networks (SARNs and LARNs) and five hydrography data products for (a) the Kotuy River, and (b) the Coleen River. SARNs show higher D_d than other Landsat-derived hydrography data products in these two basins, while the OWF of SARNs differs little from other datasets. SARNs have D_d that is 71% of NHD.

Kotuy River because GRWL only captures main rivers in the Coleen River (Figs. 7d, 8d, and 10). Surprisingly, although the resolution of G3WBM is 90 m, there is little difference between the resultant D_d and those of the existing 30 m hydrography data products (Figs. 7f, 8f, 9, 10 and Table 3).

4.3. Open water fraction analysis

In contrast to drainage density, open water fraction (OWF) of our SARNs is similar to the other datasets. The OWF values of the Kotuy and Coleen Rivers are no less than 1.05 and 1.59 times greater, respectively, than those of the other four hydrography data products (Fig. 10 and Table 3). This is because OWF is influenced primarily by the surface area of large rivers whereas smaller rivers ($\sim 1\text{--}3$ pixels wide) contribute to D_d , consistent with Allen and Pavelsky (2015). LARN OWF is approximately 30% greater than SARN OWF (Fig. 10). Because of the limitation in the Landsat-8 imagery resolution, it is difficult to distinguish the boundaries of large and small rivers from mixed pixels. As a result, all rivers that are narrower than 30 m were assigned a uniform width of 30 m, leading to overestimation of river surface area.

4.4. The longest connected river length analysis

The SARN method extracts more small rivers and significantly improves river connectivity (Figs. 7, 8 and Table 3). In the Kotuy River, the longest connected river length (L_{\max}) of SARNs is 2,512 km, and in the Coleen River, L_{\max} is 2,876 km. The L_{\max} values of SARNs in the

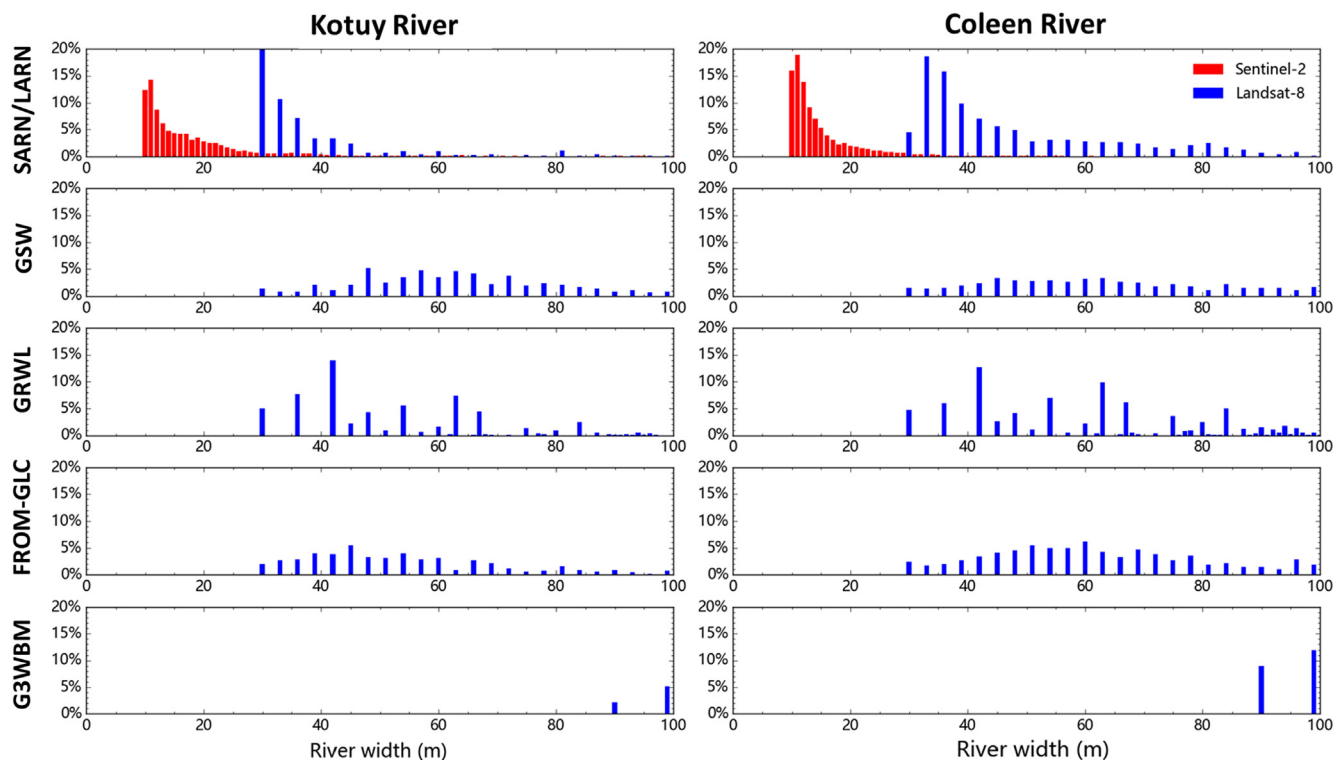


Fig. 11. River width histograms in Kotuy and Coleen Rivers. The red histograms of SARNs exhibit more small river width information as narrow as 10 m.

Kotuy and Coleen Rivers are at least 10 times greater than those of the global hydrography data products except GRWL in the Kotuy River, but less than that of NHD (Table 3). GSW and GRWL have higher L_{max} values than other global hydrography data products in the Kotuy and Coleen Rivers, respectively (Table 3). However, because GSW and GRWL only extracted large rivers, they have L_{max} approximately 80% shorter than SARNs. Therefore, merging the ArcticDEM-modeled drainage networks with Sentinel-mapped river networks can significantly improve river connectivity.

4.5. River width analysis

Rivers as narrow as 10 m can be extracted from Sentinel-2 images, providing a fully complete river width histogram as compared with Landsat-derived width distributions (Fig. 11). Of the four global hydrography data products assessed here, GRWL provides the most continuous mapping of large river widths. To assess the potential benefits of using higher resolution Sentinel-2 imagery, we selected a 2467-km² sub-basin of the Kotuy River for comparison with GRWL at the catchment scale (Fig. 12a). SARNs clearly contain more rivers that are less than 30 m wide, while the GRWL dataset only contains large rivers. The river width of SARNs positively correlates with stream order (Fig. 12b). Three tributaries in this sub-basin were selected from SARNs, and the relationship between the river width and the distance from the river basin outlet was plotted (Fig. 12). SARNs extract a higher number of small rivers with river width less than 30 m, and show negative correlation ($R^2 > 0.58, p < 0.01$) between river width and the distance from the river basin outlet (Fig. 12d, e and f). No direct correlation between the river width and distance from the basin outlet is found in GRWL (Fig. 12c). GRWL overestimates the river widths that are less than 90 m, failing to identify small rivers in mixed pixels accurately, which is consistent with a previous study (Allen and Pavelsky, 2018).

5. Discussion

This study merged 10 m resolution Sentinel-mapped rivers with

ArcticDEM-modeled rivers to extract complete and continuous river networks that included small rivers as narrow as 10 m. As compared with the National Hydrography Dataset (NHD), Sentinel-ArcticDEM merged River Networks (SARNs) are accurate and consistent for greater than 1st order NHD. Table 2 shows that this agreement worsens as rivers get larger, yet this may be due to a temporal mismatch. By comparing NHD with historical Landsat images, we determined that most of the NHD for the Coleen River were obtained before 1973 (Fig. S1), at least 40 years prior to the 2017 Sentinel-2 image used here. The highly dynamic Arctic alluvium, coupled with increasing temperatures and thawing permafrost, results in shifting thalwegs over this period, creating inconsistencies between the SARNs and NHD, especially for 6th order NHD and larger (Table 2). This finding also suggests possible obsolescence of the NHD for mapping dynamic Arctic rivers, at least in the Coleen River.

As compared with existing hydrography data products (GSW, GRWL, FROM-GLC 2017, and G3WBM) produced from 30 m Landsat series satellite imagery, SARN drainage densities are at least 4.5 times larger than other evaluated hydrography data products (Fig. 10 and Table 3), and SARNs contain much richer river width information (10–30 m) (Fig. 11). Further, our LARNs (created by imposing our method on Landsat imagery), reveal that existing hydrography data products do not fully utilize the ability of Landsat images to detect narrow water bodies because of their necessary computational simplicity for global work and the limited availability of high resolution global DEMs. Merging visible/NIR satellite imagery with ArcticDEM-modeled drainage networks better captures continuous small rivers, especially eliminating gaps from mountain shadows and bare land to maintain connectivity.

Finer resolution SARNs yield higher drainage density than LARNs, but SARNs have lower OFW than LARNs (Fig. 10). We thus conclude that surface area of rivers and streams of LARNs is overestimated. Opposite to GRWL, the river width of SARNs shows negative correlation ($R^2 > 0.58, p < 0.01$) with the distance from the river basin outlet (Fig. 12). Because of the limitation in the Landsat-8 imagery resolution, it is difficult to distinguish the boundaries of large and small rivers from

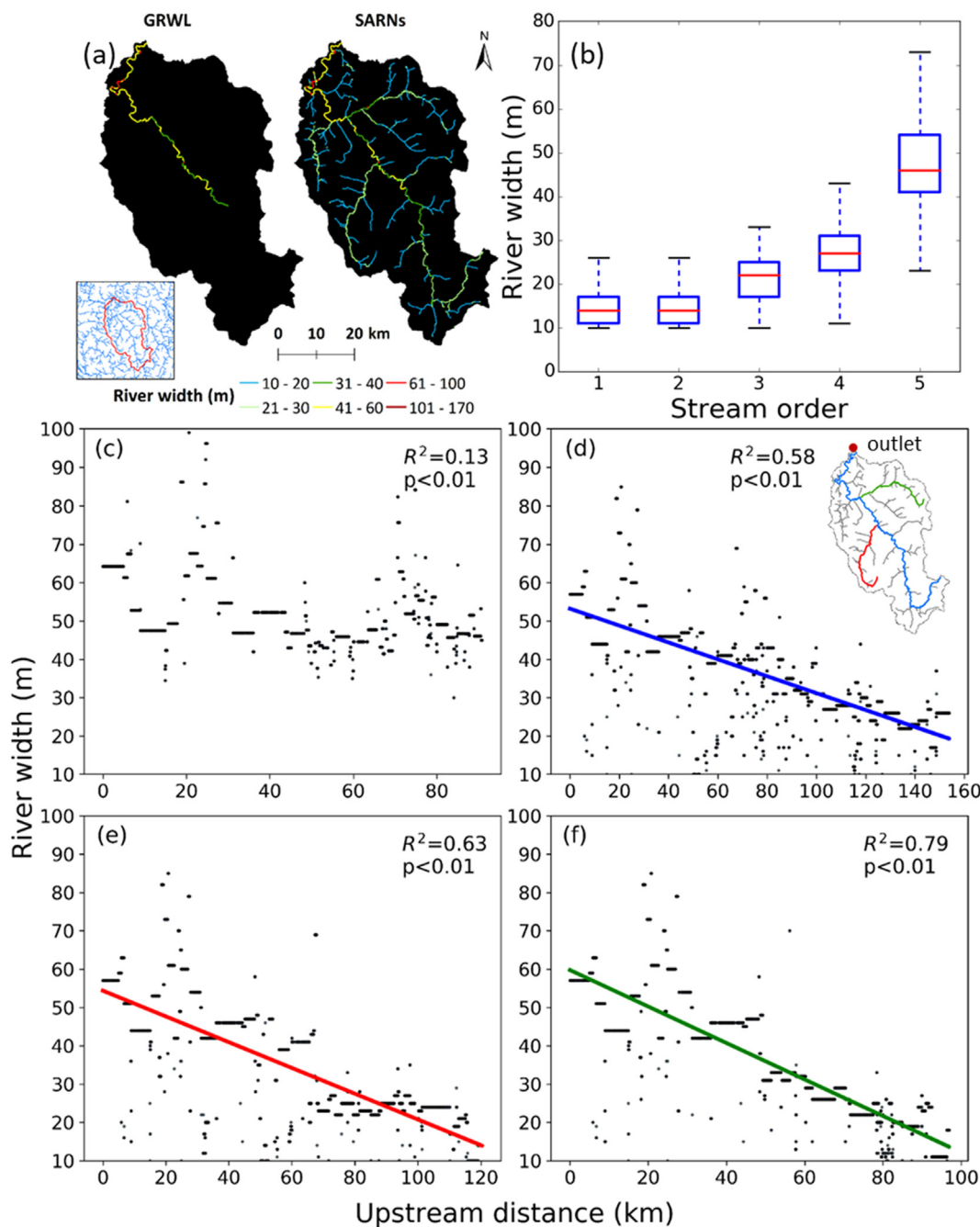


Fig. 12. River width comparisons of SARNs with GRWL in a 2467-km² sub-basin of the Kotuy River at the catchment scale. (a) is the river width distributions of SARNs and GRWL; (b) is the relationship between river width and stream order of SARNs; (c), (d), (e) and (f) are the relationship of upstream river width with distance from the river basin outlet, (c) is GRWL, while (d), (e) and (f) are three tributaries of SARNs.

mixed pixels (Crapper, 1980; Lyons et al., 2013; Yamazaki et al., 2015). Clearly, the use of Sentinel-2 images contributed to solving mixed-pixel problem, delineating the boundaries of large rivers accurately, and extracting small rivers that are 10–30 m wide.

The SARN method significantly improves river connectivity at the catchment scale. The river networks of the GSW, FROM-GLC 2017, and G3WBM datasets have low connectivity, with gap segments occurring even in large rivers, because these datasets utilize pixel-based river extraction methods (Gong et al., 2013; Pekel et al., 2016; Yamazaki et al., 2015) thus neglecting the adjacency relationship between continuous river channels. Merging Sentinel-2 with ArcticDEM topographic information delineates river networks an order of magnitude more continuous than pixel-based river network extractions alone. This in

turn can provide more information at a finer catchment scale and more correctly identify catchment properties like stream order, stream length, and other important factors (Figs. 6, 12 and Table 3).

We find three areas for improvement with the SARN method. First, some of the tundra close to river banks is difficult to remove because they are located within the river areas of interest. Future studies should seek a more effective method of removing tundra features located along river banks, for example by generating 10 m resolution Modified Normalized Difference Water Index (MNDWI) images through SWIR band sharpening (Du et al., 2016). Second, the presented SARN method requires use of several thresholds, including a low global threshold of the processed Sentinel-2 imagery to preserve the connectivity of small rivers, a low accumulation area threshold of the ArcticDEM flow

accumulation map that can cover the entire Sentinel-mapped river networks, a low-order river interest-area threshold to remove non-water features, and a high NDWI global threshold to extract large rivers. The applicability of the threshold values selected here to other locations remains untested. Third, we examined only single Sentinel-2 image here, future work should incorporate multi-temporal Sentinel-2 satellite images, in order to realize the dynamic monitoring of changes in river networks and to compensate for any lack in the temporal resolution of the NHD.

6. Conclusion

In this paper, we presented a methodology to effectively map continuous river networks from 10 m Sentinel-2 imagery with ArcticDEM data at finer reach and catchment scales. Our Sentinel-ArcticDEM merged River Networks (SARNs) align well with NHD, and their drainage densities are at least ~4.5 larger than existing Landsat-derived hydrography data products. In addition, merging remotely sensed river networks with ArcticDEM-modeled drainage networks significantly improves river connectivity with at least a ten-fold increase over the other Landsat-derived hydrography data products. The presented SARN methodology can be extended to open water extraction over the entire Arctic to produce remotely sensed Arctic river products. Growing availability of high-resolution DEMs (e.g., WorldDEM), alongside 10 m Sentinel-2 or even 3–5 m CubeSat imagery (Cooley et al., 2017; Cooley et al., 2019), portends our growing capacity to track dynamic surface water processes with unprecedented resolution over space and time.

CRediT authorship contribution statement

Xin Lu: Conceptualization, Methodology, Validation, Formal analysis, Investigation, Writing - original draft, Visualization. **Kang Yang:** Conceptualization, Methodology, Writing - review & editing, Supervision, Funding acquisition. **Yao Lu:** Validation, Formal analysis, Writing - review & editing. **Colin J. Gleason:** Validation, Writing - review & editing, Supervision. **Laurence C. Smith:** Writing - review & editing, Supervision. **Manchun Li:** Supervision, Funding acquisition.

Declaration of Competing Interest

The authors declare that they have no known competing financial interests or personal relationships that could have appeared to influence the work reported in this paper.

Acknowledgements

Kang Yang acknowledges the support of the National Key R&D Program (2018YFC1406101), the National Natural Science Foundation of China (41871327), and the Fundamental Research Funds for the Central Universities.

Appendix A. Supplementary data

Supplementary data to this article can be found online at <https://doi.org/10.1016/j.jhydrol.2020.124689>.

References

- Aires, F., et al., 2018. Comparison of visible and multi-satellite global inundation datasets at high-spatial resolution. *Remote Sens. Environ.* 216, 427–441. <https://doi.org/10.1016/j.rse.2018.06.015>.
- Ala-Aho, P., et al., 2018. Using stable isotopes to assess surface water source dynamics and hydrological connectivity in a high-latitude wetland and permafrost influenced landscape. *J. Hydrol.* 556, 279–293. <https://doi.org/10.1016/j.jhydrol.2017.11.024>.
- Allen, G.H., Pavelsky, T.M., 2015. Patterns of river width and surface area revealed by the satellite-derived North American River Width data set. *Geophys. Res. Lett.* 42 (2), 395–402. <https://doi.org/10.1002/2014gl062764>.
- Allen, G.H., Pavelsky, T.M., 2018. Global extent of rivers and streams. *Science* 361, 585–588. <https://doi.org/10.1126/science.aat0636>.
- Allen, G.H., et al., 2018. Similarity of stream width distributions across headwater systems. *Nat. Commun.* 9 (1), 610. <https://doi.org/10.1038/s41467-018-02991-w>.
- Alsdorf, D.E., Rodríguez, E., Lettenmaier, D.P., 2007. Measuring surface water from space. *Rev. Geophys.* 45 (2). <https://doi.org/10.1029/2006RG000197>.
- Anderson, L., Birks, J., Rover, J., Guldager, N., 2013. Controls on recent Alaskan lake changes identified from water isotopes and remote sensing. *Geophys. Res. Lett.* 40 (13), 3413–3418. <https://doi.org/10.1002/grl.50672>.
- Baillarin, S.J., et al., 2012. Sentinel-2 level 1 products and image processing performances, IEEE International Geoscience and Remote Sensing Symposium. IEEE. DOI:10.1109/igass.2012.6351959.
- Bajjali, W., 2018a. ArcScan, ArcGIS for Environmental and Water Issues. Springer, pp. 89–102.
- Bajjali, W., 2018b. Watershed Delineation, ArcGIS for Environmental and Water Issues. Springer, pp. 235–245.
- Benstead, J.P., Leigh, D.S., 2012. An expanded role for river networks. *Nat. Geosci.* 5 (10), 678–679. <https://doi.org/10.1038/ngeo1593>.
- Bliss, T., 1981. Tundra ecosystems: a comparative analysis, 25. CUP Archive.
- Brabets, T.P., Wang, B., Meade, R.H., 2000. Environmental and hydrologic overview of the Yukon River Basin, Alaska and Canada.
- Brown, J., Ferrians Jr, O., Heginbottom, J., Melnikov, E., 1997. Circum-Arctic Map of Permafrost and Ground-ice Conditions. US Geological Survey Reston, VA.
- Butman, D., et al., 2016. Aquatic carbon cycling in the conterminous United States and implications for terrestrial carbon accounting. *Proc. Natl. Acad. Sci.* 113 (1), 58–63. <https://doi.org/10.1073/pnas.1512651112>.
- Chen, M., Rowland, J.C., Wilson, C.J., Altmann, G.L., Brumby, S.P., 2014. Temporal and spatial pattern of thermokarst lake area changes at Yukon Flats, Alaska. *Hydrol. Processes* 28 (3), 837–852. <https://doi.org/10.1002/hyp.9642>.
- Cooley, S., Smith, L., Stepan, L., Mascaro, J., 2017. Tracking dynamic northern surface water changes with high-frequency planet CubeSat imagery. *Remote Sensing* 9 (12), 1306. <https://doi.org/10.3390/rs9121306>.
- Cooley, S.W., Smith, L.C., Ryan, J.C., Pitcher, L.H., Pavelsky, T.M., 2019. Arctic-boreal lake dynamics revealed using CubeSat imagery. *Geophys. Res. Lett.* 46 (4), 2111–2120. <https://doi.org/10.1029/2018gl081584>.
- Crapper, P., 1980. Errors incurred in estimating an area of uniform land cover using Landsat Photogramm. *Eng. Remote Sens.*
- Czuba, J.A., Foufoula-Georgiou, E., 2015. Dynamic connectivity in a fluvial network for identifying hotspots of geomorphic change. *Water Resour. Res.* 51 (3), 1401–1421. <https://doi.org/10.1002/2014WR016139>.
- Dai, C., Durand, M., Howat, I.M., Altenau, E.H., Pavelsky, T.M., 2018. Estimating river surface elevation from ArcticDEM. *Geophys. Res. Lett.* 45 (7), 3107–3114. <https://doi.org/10.1002/2018GL077379>.
- Downing, J.A., et al., 2012. Global abundance and size distribution of streams and rivers. *Inland Waters* 2 (4), 229–236. <https://doi.org/10.5268/IW-2.4.502>.
- Drusch, M., et al., 2012. Sentinel-2: ESA's optical high-resolution mission for GMES operational services. *Remote Sens. Environ.* 120, 25–36. <https://doi.org/10.1016/j.rse.2011.11.026>.
- Du, Y., et al., 2016. Water bodies' mapping from sentinel-2 imagery with modified normalized difference water index at 10-m spatial resolution produced by sharpening the SWIR band. *Remote Sens.* 8 (4), 354. <https://doi.org/10.3390/rs8040354>.
- Fairfield, J., Leymarie, P., 1991. Drainage networks from grid digital elevation models. *Water Resour. Res.* 27 (5), 709–717. <https://doi.org/10.1029/90wr02658>.
- Feng, D., Gleason, C.J., Yang, X., Pavelsky, T.M., 2019. Comparing discharge estimates made via the BAM algorithm in high-order Arctic rivers derived solely from optical CubeSat, Landsat, and Sentinel-2 data. *Water Resour. Res.* 55 (9), 7753–7771. <https://doi.org/10.1029/2019WR025599>.
- Feyisa, G.L., Meilby, H., Fenstholm, R., Proud, S.R., 2014. Automated Water Extraction Index: a new technique for surface water mapping using Landsat imagery. *Remote Sens. Environ.* 140, 23–35. <https://doi.org/10.1016/j.rse.2013.08.029>.
- Gleason, C.J., Smith, L.C., 2014. Toward global mapping of river discharge using satellite images and at-many-stations hydraulic geometry. *Proc. Natl. Acad. Sci.* 111 (13), 4788–4791. <https://doi.org/10.1073/pnas.1317606111>.
- Godsey, S.E., Kirchner, J.W., 2014. Dynamic, discontinuous stream networks: hydrologically driven variations in active drainage density, flowing channels and stream order. *Hydrol. Process.* 28 (23), 5791–5803. <https://doi.org/10.1002/hyp.10310>.
- Gong, P., et al., 2013. Finer resolution observation and monitoring of global land cover: first mapping results with Landsat TM and ETM+ data. *Int. J. Remote Sens.* 34 (7), 2607–2654. <https://doi.org/10.1080/01431161.2012.748992>.
- Goodchild, M.F., Hunter, G.J., 1997. A simple positional accuracy measure for linear features. *Int. J. Geograph. Inf. Sci.* 11 (3), 299–306. <https://doi.org/10.1080/136588197242419>.
- Jung, M., et al., 2010. Recent decline in the global land evapotranspiration trend due to limited moisture supply. *Nature* 467 (7318), 951–954. <https://doi.org/10.1038/nature09396>.
- Kenward, T., 2000. Effects of digital elevation model accuracy on hydrologic predictions. *Remote Sens. Environ.* 74 (3), 432–444. [https://doi.org/10.1016/s0034-4257\(00\)00136-x](https://doi.org/10.1016/s0034-4257(00)00136-x).
- Lehner, B., Verdin, K., Jarvis, A., 2006. HydroSHEDS technical documentation, version 1. 0. World Wildlife Fund US, Washington, DC, pp. 1–27.
- Li, J., Wong, D.W.S., 2010. Effects of DEM sources on hydrologic applications. *Comput. Environ. Urban Syst.* 34 (3), 251–261. <https://doi.org/10.1016/j.compenvurbsys.2009.11.002>.
- Lyons, E.A., et al., 2013. Quantifying sources of error in multitemporal multisensor lake mapping. *Int. J. Remote Sens.* 34 (22), 7887–7905. <https://doi.org/10.1080/01431161.2013.827343>.
- McCabe, M.F., et al., 2017. The future of Earth observation in hydrology. *Hydrol. Earth*

- Syst. Sci. 21 (7), 3879–3914. <https://doi.org/10.5194/hess-21-3879-2017>.
- McFeeters, S.K., 1996. The use of the Normalized Difference Water Index (NDWI) in the delineation of open water features. Int. J. Remote Sens. 17 (7), 1425–1432. <https://doi.org/10.1080/01431169608948714>.
- Meyer, J.L., et al., 2007. The contribution of headwater streams to biodiversity in river networks. JAWRA J. Am. Water Res. Assoc. 43 (1), 86–103. <https://doi.org/10.1111/j.1752-1688.2007.00008.x>.
- Morin, P., et al., 2016. ArcticDEM; a publically available, high resolution elevation model of the Arctic. EGU General Assembly Conference Abstracts.
- O'Callaghan, J.F., Mark, D.M., 1984. The extraction of drainage networks from digital elevation data. Computer Vision, Graphics, Image Process. 28 (3), 323–344.
- Pekel, J.-F., Cottam, A., Gorelick, N., Belward, A.S., 2016. High-resolution mapping of global surface water and its long-term changes. Nature 540 (7633), 418–422. <https://doi.org/10.1038/nature20584>.
- Peterson, B.J., 2001. Control of nitrogen export from watersheds by headwater streams. Science 292 (5514), 86–90. <https://doi.org/10.1126/science.1056874>.
- Raymond, P.A., et al., 2013. Global carbon dioxide emissions from inland waters. Nature 503 (7476), 355–359. <https://doi.org/10.1038/nature12760>.
- Seybold, H., Rothman, D.H., Kirchner, J.W., 2017. Climate's watermark in the geometry of stream networks. Geophys. Res. Lett. 44 (5), 2272–2280. <https://doi.org/10.1002/2016gl072089>.
- Shiklomanov, A.I., Lammers, R.B., Vörösmarty, C.J., 2002. Widespread decline in hydrological monitoring threatens pan-Arctic research. Eos, Trans. Am. Geophys. Union 83 (2), 13–17. <https://doi.org/10.1029/2002EO000007>.
- Simley, J., Carswell Jr, W., 2009. The National Map—Hydrography: US Geological Survey Fact Sheet 2009–3054. US Geological Survey National Center, Reston, VA.
- Sjögersten, S., et al., 2014. Tropical wetlands: a missing link in the global carbon cycle? Global Biogeochem. Cycles 28 (12), 1371–1386. <https://doi.org/10.1002/2014GB004844>.
- Smith, L.C., 1997. Satellite remote sensing of river inundation area, stage, and discharge: a review. Hydrol. Process. 11 (10), 1427–1439.
- Strahler, A.N., 1957. Quantitative analysis of watershed geomorphology. Eos, Trans. Am. Geophys. Union 38 (6), 913. <https://doi.org/10.1029/tr038i006p00913>.
- Usgs, U., 2001. HYDRO1k Elevation Derivative Database. US Geological Survey Washington, DC.
- Verpoorter, C., Kutser, T., Tranvik, L., 2012. Automated mapping of water bodies using Landsat multispectral data. Limnol. Oceanogr. Methods 10 (12), 1037–1050. <https://doi.org/10.4319/lom.2012.10.1037>.
- Vorosmarty, C.J., 2000. Global water resources: vulnerability from climate change and population growth. Science 289 (5477), 284–288. <https://doi.org/10.1126/science.289.5477.284>.
- Xu, H.-Q., 2005. A study on information extraction of water body with the modified normalized difference water index (MNDWI). J. Remote Sens. 5, 589–595.
- Yamazaki, D., et al., 2017. A high-accuracy map of global terrain elevations. Geophys. Res. Lett. 44 (11), 5844–5853. <https://doi.org/10.1002/2017gl072874>.
- Yamazaki, D., Trigg, M.A., Ikeshima, D., 2015. Development of a global ~90m water body map using multi-temporal Landsat images. Remote Sens. Environ. 171, 337–351. <https://doi.org/10.1016/j.rse.2015.10.014>.
- Yang, K., et al., 2014. River delineation from remotely sensed imagery using a multi-scale classification approach. IEEE J. Sel. Top. Appl. Earth Obs. Remote Sens. 7 (12), 4726–4737. <https://doi.org/10.1109/jstars.2014.2309707>.
- Yang, K., et al., 2015. River detection in remotely sensed imagery using gabor filtering and path opening. Remote Sensing 7 (7), 8779–8802. <https://doi.org/10.3390/rs70708779>.